Upwelling in Cyclonic and Anticyclonic Eddies at the Middle Atlantic Bight Shelf-Break Front

Andrew J. Hirzel[1*], Weifeng (Gordon) Zhang[2], Glen G. Gawarkiewicz[2], Dennis J. McGillicuddy Jr.[2]

[1] Massachusetts Institute of Technology/Woods Hole Oceanographic Institution Joint Program in Oceanography/Applied Ocean Science and Engineering, 266 Woods Hole Rd, Woods Hole, MA, 02543, USA
[2] Woods Hole Oceanographic Institution, 266 Woods Hole Rd, Woods Hole, MA, 02543, USA

Corresponding Author:
Andrew Hirzel
ahirzel@hawaii.edu
C-MORE Hale, 1950 East West Road, Honolulu, HI, 96822

[*] Present Address: University of Hawai‘i at Mānoa, 2500 Campus Rd, Honolulu, HI 96822

Key Points

- Two frontal eddies of opposite rotational directions were observed at the Middle Atlantic Bight shelf-break front.
- Nutrients, chlorophyll, diatom chains, and small copepods were enhanced in the eddies.
- Model simulation was consistent with upwelling within both features.

Abstract

Despite the ubiquity of eddies at the Mid-Atlantic Bight shelf-break front, direct observations of frontal eddies at the shelf-break front are historically sparse and their biological impact is mostly unknown. This study combines high resolution physical and biological snapshots of two frontal eddies with an idealized 3-D regional model to investigate eddy formation, kinematics, upwelling patterns, and biological impacts. During May 2019, two eddies were observed in situ at the shelf-break front. Each eddy showed evidence of nutrient and chlorophyll enhancement despite rotating in opposite directions and having different physical characteristics. Our results suggest that cyclonic eddies form as shelf waters are advected offshore and slope waters are advected shoreward, forming two filaments that spiral inward until sufficient water is entrained. Rising isohalines and upwelled slope water dye tracer within the model suggest that upwelling coincided with eddy formation and persisted for the duration of the eddy. In contrast, anticyclonic eddies form within troughs of the meandering shelf-break front, with amplified frontal meanders creating recirculating flow. Upwelling of subsurface shelf water occurs in the form of detached cold pool waters during the formation of the anticyclonic eddies. The stability properties of each eddy type were estimated via the Burger number and suggest different ratios of baroclinic versus barotropic contributions to frontal eddy formation. Our observations and model results indicate that both eddy types may persist for more than a month and upwelling in both eddy types may have significant impacts on biological productivity of the shelf break.

Plain Language Summary

The Middle Atlantic Bight shelf-break front is a highly variable region that frequently forms frontal eddies. In situ observations of the physical and biological characteristics of these eddies are relatively scarce. We present observations of two eddies, each of which showed evidence of nutrient and chlorophyll enhancement despite having drastically different characteristics and different formation processes. Satellite data indicate that neither of the two types of eddies are rare, indicating a potential for frontal eddies to significantly influence biological communities near the front.

1. Introduction

The Middle Atlantic Bight (MAB) shelf-break front is characterized by its variability, with its physical, biological, and chemical attributes varying significantly in both time and space (Linder and Gawarkiewicz, 1998; Loder et al., 2001; Zhang et al., 2011). The front separates two water masses: cold, fresh shelf water inshore and warm, salty Slope Sea water offshore. In warm seasons (late spring to fall), a prominent body of near-bottom cold water – the cold pool – resides on the shelf side of the front as a remnant of winter-cooled shelf water and is bounded above by the seasonal thermocline (Houghton et al., 1982; Lentz, 2017). Like many other oceanic frontal regions (e.g., Munk et al., 2000), eddies are common at the MAB shelf-break front. Satellite imagery frequently shows eddies arrayed across the extent of the shelf-break front, e.g., in May 1982 (Garvine et al., 1988, Figure 1), May 1980 and 1984 (Ryan et al., 1999a, Figure 2), and May 1997 (Ryan et al., 1999b, Plate 1). These frontal eddies may be formed through frontal instabilities (Garvine et al., 1988; Houghton et al., 1986) or by external forcing, such as Gulf

Stream warm-core rings (e.g., Kennelly et al., 1985). Successive frontal meander troughs and crests may have completely different hydrodynamic balances (Pickart, 1999), which can result in mesoscale and submesoscale patches of high vorticity on either side of the shelf-break front (Zhang and Gawarkiewicz, 2015). These differing characteristics mean that frontal meandering can lead to formation of eddies of varying rotational direction or water mass characteristics.

However, despite the ubiquity of eddies at the shelf-break front, direct observations of frontal eddies at the MAB shelf-break front are historically sparse, particularly when not influenced by Gulf Steam warm-core rings. Garvine et al. (1988) described two cyclonic slope water eddies, along with a possible offshore anticyclonic slope water eddy. Both of the cyclonic eddies were observed drawing shelf water offshore, across the front. Houghton et al. (1986) observed a shelf water filament being drawn offshore, which instead formed an anticyclonic shelf water eddy seaward of the front. Gawarkiewicz et al. (2001) observed an anticyclonic slope water eddy, which was estimated to contain variable upwelling and downwelling. Flagg et al. (1997) observed a series of anticyclonic "cold pool" eddies, which were associated with increased chlorophyll. The above list represents the majority of studies directly focused on MAB frontal eddies. However, frontal eddies in other regions have long been recognized as an important vector for cross-frontal water exchange, during which they may also upwell nutrients and impact local productivity (e.g., Pingree, 1978; 1979, in the Celtic Sea).

This study describes the kinematics of two frontal eddies originating on opposites sides of the front, one cyclonic and one anticyclonic. Satellite imagery and in situ observations are used to track the eddies over time. Model results are then used to investigate the kinematic evolution of the eddies and to describe the associated upwelling patterns, with the intent of determining the possible impact of frontal eddies on biological processes. The dynamics of eddy formation will be investigated in future studies.

2. Materials and Methods

2.1 Observations

Direct observations of two eddies occurred during a two-week cruise in May of 2019 (*NOAAS Ronald H. Brown* voyage RB19-04, May 12-25). The sampling was primarily along a cross-shelf transect south of Cape Cod, MA (Figure 1, first row). Additional measurements were collected west of the transect line as eddies moved off of the main transect line. The 34.5 isohaline was used to identify the location of the shelf-break front, following the convention of previous studies (e.g., Beardsley and Flagg, 1976; Chen and He, 2010; Linder and Gawarkiewicz, 1998). Waters further on shelf are less than 34 and waters further offshore are greater than 35, so the location of the 34.5 isohaline provides a useful indication of mixing between the shelf and slope waters (i.e., the front). Transect crossings spanning multiple year-days are labelled herein as a year-day span (e.g., year-day 132-133).

Station profiles were measured by a Seabird SBE 911+ (conductivity, temperature, and pressure) and a WetLabs FLNTURTD fluorometer (chlorophyll fluorescence) mounted upon a rosette. Seawater samples were taken at discrete depths with 24 10 L Niskin bottles mounted on the rosette. Nitrate, phosphate, and silicate concentration in samples were processed in the Woods Hole Oceanographic Institution Nutrient Analytical Facility. Plankton were imaged with a Digital Auto Video Plankton Recorder (DAVPR, from SeaScan Inc.) mounted upon the CTD

rosette. The DAVPR included a Seabird Electronics Inc. CTD (SBE 49 FastCat), fluorometer (FLNTURTD-4620), and synchronized video camera and xenon strobe (Davis et al., 2004). Both CTD and DAVPR measurements were averaged into 1 m depth bins. DAVPR video frame frequency and dimensions were 20 Hz and 1392 x 1040 pixels (~10 x 7 x 25 mm volume imaged) respectively. Higher resolution physical and biological parameters were sampled with a towed Video Plankton Recorder II (VPRII, from SeaScan Inc.). The VPRII consists of a towed body, containing a Seabird Electronics Inc. CTD (SBE 49 FastCat), oxygen sensor (SBE 43), fluorometer (ECO FLNTU-4050), ECO Triplet (ECO BBFL2-123), PAR (photosynthetically active radiation; Biospherical Instruments Inc. QCP-200L), and synchronized video camera and xenon strobe (Davis et al., 2005). The VPRII was towed at 10 knots (5.1 m s^{-1}), undulating between depths of 5 m and 100 m approximately every 6 minutes. Plankton video frames for the DAVPR and VPRII were captured at 20 Hz and 30 Hz respectively. DAVPR video frame dimensions were 1392 x 1040 pixels (~10 x 7 x 25 mm volume imaged) and VPRII video frame dimensions were 1380 x 1034 pixels (~20 x 15 x 23 mm volume imaged). Individual video frames from both instruments were passed through object identification software to identify "regions of interest" (ROIs), which were then saved to disk with a time-stamp naming convention (Davis et al., 2004). ROIs were manually annotated to the highest level of taxonomic identification possible based on imagery alone. Herein we focus our analysis on the most abundant categories (i.e., diatom chains, small copepods). Manually annotated DAVPR ROIs are used for all diatom and copepod results presented in the figures of the main body of this paper. VPRII planktonic results are only shown in supplemental material (i.e., Supplemental Figure 5). VPRII planktonic result images were classified using a Convolutional Neural Network following the procedure described in Hirzel (2023).

2.2 Model Description

This study used an idealized 3-dimensional frontal model developed by Zhang and Gawarkiewicz (2015) to provide insight into the behavior of both types of frontal eddies. Briefly, the model was based on the Regional Ocean Modeling System (Shchepetkin and McWilliams, 2008). The model domain was rectangular, with the span of 2010 and 479 km in the along-shelf (x) and cross-shelf (y) directions, respectively. Bathymetry was uniform in the along-shelf direction and varied only in the cross-shelf direction. The model had a horizontal resolution of 500 m and 60 terrain-following vertical (sigma) layers. Temperature and salinity were initialized based on wintertime climatological conditions in the New England shelf-break region. The initial velocity field was determined by thermal-wind balance with zero bottom velocity. This yielded a shelf-break front with strong gradients in both temperature and salinity, as well as a westward frontal jet in the model initial condition (Figure 1). This climatology was persisted along the upstream (eastern) boundary. Throughout the integration, the eastern 700 km of the model domain was nudged to these same climatological conditions in order to maintain steady upstream inflow. The downstream (western) boundary was left open and a 156-km-wide offshore deep-sea region acted as a sponge layer to minimize wave reflection. Results were analyzed in a 250x60 km interior subdomain, far enough removed from the boundaries for the solution to evolve freely.

Meteorological conditions observed at the New England shelf break in April to May 2018 were used to perturb the front and were applied in a spatially uniform manner, in light of the fact that the length scale of variability in meteorological forcing is generally much larger than the length scale of the shelf break front. There are circumstances in which the local oceanography modulates air-sea fluxes (e.g., Dewar, 1986; Spall et al., 2016; Williams, 1988). However, we focus here on eddy formation due to the internal stability of the front and assume that spatial variations in surface fluxes are a second order effect.

The model was started in April because spinup time was required to transition from the initial climatological state to the dynamic environment present at the front when our observations were taken in May. Air temperatures below 10°C were increased to 10°C, in order to remove surface-cooling-induced convective mixing that did not occur in the ocean during our cruise period. Modelled dye tracers were used to explore upwelling. Two subsurface dyes were introduced within the model domain at the beginning of the simulation, one inshore and one offshore of the shelf-break front, to represent shelf and slope waters respectively (Figure 1). Dye concentrations in the top 100 m were initialized to be the same values as the depth, i.e., concentrations increased linearly from 0 at the surface to 100 at 100 m. Below 100 m, dye concentrations were initialized at 100. During model evolution, vertical mixing of the dyes was turned off. All other parameters experienced full mixing. Because the numerical mixing is negligible during the short-term simulation, changes in modelled dye distribution were caused mostly by horizontal and vertical advection. Therefore, upwelling and downwelling were indicated at any locations where a dye concentration was greater or lesser than the initial value at a specified depth, respectively. Shelf dye and slope dye were separated by the 34.5 isohaline. To avoid sharp gradients in the dye concentrations, the frontal transitions of both dyes were smoothened within a cross-shelf distance of 10 km.

3. Results

3.1 Shipboard and satellite observations

Two frontal eddies were evident in our in situ observations: Eddy A, a cyclonic eddy that was located seaward of the shelf-break front, and Eddy B, an anticyclonic eddy that was located shoreward of the front (Table 1, Figure 2). Eddy A was characterized by a surface spiral pattern, formed of two filaments, one originating from shelf waters and one from slope waters (Figure 2 left column, Supplemental Figure 1). The filament of warm and salty slope water originated from the southeast of our main transect (Figure 3, year-days 129 and 131). This slope water filament extended northwestward to the north of a cold and fresh shelf filament extending southeastward from shelf waters. Both of these filaments extended to roughly 70 m in depth and were located above deeper slope waters (Figure 2, Figure 4). Velocities within both filaments extended deeper than their water mass and biogeochemical anomalies, down to 100 m depth. When last sampled (Figure 5), both filaments had coalesced. Coalesced waters were relatively cooler and fresher at the surface and became warmer and saltier with depth. This coalescence, combined with frequent cloud cover, prevented distinguishment of Eddy A from surrounding slope waters in subsequent satellite observations. Satellite SST showed approximately 10 days passed between when the slope filament began to extend inshore and when the shelf and slope filaments coalesced (Figure 3). Velocities in the eddy region were strongest in the east-west direction (~0.4 m s^{-1}), with

weaker north-south velocities while forming (Figure 4 third and fourth rows) and after the cyclonic eddy had formed (Figure 5). Nutrient enhancement was observed in the surface layer of the eddy compared to surrounding waters for nitrate (Figure 2, 4), phosphate, and silicate (Supplemental Figure 4), implying upwelling. When first observed on year-day 132-133, the slope filament showed a complex vertical structure in nitrate, appearing to have a local minimum around 30-40 m in depth (Figure 4). This local minimum is not present in later transects (Figure 4, year-days 135 and 137) and is discussed in Section 4.1. Surface nitrate declined after coalescence but was still elevated relative to surrounding shelf and slope waters (Figure 5). Chlorophyll inside the eddy was initially similar to surrounding waters and increased within both filaments by year-day 137 (Figure 4, fifth row). Chlorophyll was highest within the eddy once the filaments had coalesced (Figure 5). Diatom chains measured with the VPR were primarily associated with shelf waters, i.e., the shelf filament (e.g., year-day 135) (Figure 4 seventh row, Supplemental Figure 5 first column) and surface waters after coalescence (Figure 5). Small copepod abundance was more variable, but roughly mirrored diatom distributions and was enhanced within eddy center after coalescence (Figure 4 last row, Supplemental Figure 5 second column).

Eddy B was primarily characterized by a core of cold pool waters (<7.5°C) surrounded by relatively warmer (9-10°C), saltier (33.2-33.7 PSU) shelf waters more characteristic of waters typically found closer to the shelf-break front (Figure 2 right column, Figure 6). We have used the term "near-frontal" hereafter to describe the surrounding waters since the water mass is below 34 PSU, which is commonly used as the upper bound for shelf waters (e.g., Lentz, 2003). A thin lens (~10m) of warmer waters at the surface covered the deeper, colder waters in all transects. Eddy B had little surface expression in satellite imagery as a result (Figure 3) but could be delineated to the east by a relatively warm filament of near-frontal warmer and saltier shelf waters intruding into the surrounding cooler shelf waters. This filament began extending westward from year-day 141 along the northern boundary of Eddy B until it was last distinguishable in satellite imagery on year-day 144 (Figure 3 labelled on year-day 144, Supplemental Figure 1). Slope waters bounded Eddy B to the west. To the south, Eddy B was bordered by warmer, saltier shelf waters, which extended roughly 10-20 km southward before reaching the front for the duration that Eddy B was observed (Figures 2, 6; Supplemental Figure 2). The warm and salty shelf waters to the south of the eddy were roughly 30 m in depth, overlaying slope waters and located between the cold pool core of Eddy B and the front. The vertical extent of these waters declined to roughly 15 m depth by year-day 144 (Figure 6) as these waters moved west (Figure 3). Like Eddy A, east-west velocities associated with Eddy B (~0.2 m s^{-1}) were larger than the north-south component (Figure 6 third and fourth rows). A VPRII survey of Eddy B on year-day 143 revealed a longitudinal extent of over 20 km, with a latitudinal extent of roughly 10 km (Figure 7). Like Eddy A, Eddy B contained enhanced nutrients in its center (Figure 6 sixth row). Unlike Eddy A, chlorophyll was highest within the periphery of Eddy B (Figure 6 fifth row), in the warmer and saltier shelf waters present both to the north and to the south of eddy center. Diatoms and copepods measured by the VPR were both highest within the center of Eddy B (Figure 6 last two rows, year-days 142-143, 144).

Both eddies appeared to have formed at the front. Neither eddy crossed the shelf-break front while observed in situ or through satellite imagery. Both eddies moved westward along the front for the duration of the cruise, with Eddy B traveling roughly twice as fast as Eddy A.

3.2 Model Output and Interpretation

Our model is able to simulate features similar to those of Eddy A and Eddy B (Table 1, Figure 8). Four eddies similar to Eddy A and three eddies similar to Eddy B (Eddies mA1-mA4 and mB1-mB3 respectively) are identified and followed over time. Model eddies of each type are qualitatively similar in physical characteristics (e.g., size, shape, structure) and development, and so only one model eddy of each type (mA2 and mB2) will be discussed in detail. Formation of a shallow mixed layer, composed of primarily shelf waters over slope waters, occurs during the initial slumping of the shelf-break front (prior to model day 10) due to offshore Ekman transport driven by eastward winds. This change does not appear to influence formation of either type of eddy or surface spiral patterns similar to those observed in Eddy A. The primary impact of this layer is that surface salinities are lower than would be expected, such that what we refer to as a "slope water filament" has salinities of less than 34.5 within the mixed layer. For ease of interpretation, we will primarily focus on interpretation of model output below this mixed layer (i.e., at 30 m in depth).

The model Eddy mA2 develops similarly to that of our observed Eddy A (Figures 8, 9, 10). Eddy mA2 begins forming after frontal meanders have formed (Figure 9 first row, Figure 10 column 1). Increased frontal meander amplitude causes the front to roll over, advecting slope water onshore and advecting shelf water offshore (Figure 9 second row, Figure 10 column 2). As time passes, the front continues to roll up, causing both filaments to continue spiraling inward (Figure 10 column 3). As more shelf and slope waters spiral inward, the entrained fluid increases the size of the eddy (Figure 9 third row, Figure 10 column 4). The two filaments also decrease in width. The spiral pattern shown by slope dye concentrations persists longer than the salinity spiral, as slope dye concentrations are only influenced by advection due to explicit mixing (e.g., vertical diffusion) of the dye tracer being turned off. Eddy mA2 continues to be visible for the duration of the simulation (60 days) and forms subsequent spirals. Spiral creation time in the model is approximately equal to that of observations, with the first spirals in eddies mA1-mA4 forming and evolving over the course of 12 model days and a successive set of spirals forming and evolving over 10 model days.

Upwelling of slope water dye starts at the front to the west of Eddy mA2 (model day 10, Figure 10 third and fourth rows). Shelf water is entrained from the western side of the eddy and slope water is entrained from the eastern side, developing into a clear spiral pattern (Figure 10, model days 16-22). Slope dye concentrations within the eddy increase over time indicating that deeper slope waters are entrained with the movement of shelf waters. The upwelling flow intensifies as the frontal meander increases in magnitude. Isohalines at eddy center rise and stay domed throughout the spiral and eddy formation (Figure 10, second row). Shelf water dye is not elevated within shelf filaments or the eddy beyond concentrations expected by horizontal advection (not shown; only slope dye is shown in Figure 10), indicating that upwelling is predominately of deeper slope waters within Eddy mA2 (Figure 10, last row). For a fixed volume, continuity would imply that inward-spiraling filaments should yield downwelling within

the eddy center, but we saw no evidence of systematic downwelling in the eddy (Figure 10). Instead, the size of Eddy mA2 increases as upwelled fluid is entrained, and that appears to counterbalance any downwelling implied by an inward spiral.

Model eddies mA1, mA3, and mA4 mostly vary from Eddy mA2 in terms of quantity of shelf water advected, which then alters the shapes of the developing spirals and eddies (Figure 8). Little is affected regarding the occurrence, date, or duration of formation of either the initial spiral patterns or later formation of the cyclonic eddies. Subsequent spirals are observed forming associated with meander crests – during the one instance where an eddy departs from the meander crest (Figure 8, Eddy mA3, model day 19), the eddy resulting from the previous spiral is entrained by the newly forming spiral pattern (model-day 22). After this, Eddy mA3 remains within the meander crest and formed subsequent spirals, similar to Eddies mA1, mA2, and mA4.

The model Eddy mB2 is an anticyclonic eddy with a core of cold pool waters, similar to what we observed for Eddy B (Figures 8, 9, and 11). Eddy mB2 formation begins within the frontal trough between Eddies mA2 and mA3 (Figure 9 first row, Figure 11 first row). As the meanders increase in amplitude (Figure 11 column 2), irregularities within the front result in the frontal jet travelling more northward (Figure 11 column 3), which later results in shelf waters traveling to the east (Figure 9 second row, Figure 11, column 4). Velocities are initially variable in depth and intensity. Over time, a more coherent flow develops, creating an anticyclonic eddy, with velocities extending throughout the upper 100-150 m of the water column (Figure 9 third row, Figure 11 column 5). Once this has occurred, Eddy mB2 decouples from surrounding eddies (i.e., leaves the trough between cyclonic eddies) and travels along the front. Eddy mB2 travels westward more rapidly than model eddies mA1-mA4 and is to the immediate north of Eddy mA2 on model day 39 (Figure 8 last row, Figure 11 column 5). Unlike Eddy mA2, upwelling was not continuous during and after the formation of Eddy mB2. Instead, a parcel of cold pool water rises along the front into the developing meander and the cold pool water parcel is then separated from inshore shelf waters as Eddy mB2 forms (Figure 9 right column, Figure 11 last row). Once the cold pool water parcel detaches from its origin, the encircling warmer and saltier waters prevent replenishment or further enhancement.

Model features similar to Eddy B do not all persist on the same side of the shelf-break front as they formed, unlike those similar to Eddy A (Figure 8). Modelled Eddy mB2, described above, is the most similar to the observed Eddy B, in that it remains near to the front and seaward of the front. Modelled Eddy mB1 also forms a persisting anticyclonic eddy with detached cold pool waters in its core, but it travels across the front post-formation (Figure 8, last row, far left). Eddy mB1 then proceeds farther south into the Slope Sea, possibly as a result of Eddy mA2 being in close proximity to the immediate east of Eddy mB1. The salinity is higher within Eddy mB1 compared to Eddy mB2. Eddy mB3 never intensifies into a full eddy, nor do its core cold pool waters fully detach from inshore waters. This incomplete formation is likely due to both forming in a lower-amplitude frontal trough and the presence of a cyclonic shelf water eddy nearby. The end result is that Eddy mB3 is transient, unlike the other model eddies.

4. Discussion

4.1 Eddy A

298 Our model eddies mA1-mA4 replicated surface spiral patterns that developed similarly to
299 those observed in SST observations and replicated cross-shelf profiles similar to those measured
300 in situ for Eddy A. Modelled eddy diameters were slightly larger (18.75±1.5 km) than observed
301 Eddy A (15 km) and had greater depths (125±10 m vs. 70 m) (Table 1). Modelled and observed
302 maximum azimuthal velocities were similar, all ~0.4 m s^{-1}. Modelled westward translational
303 speeds were slightly slower (2.98±0.7 km day^{-1}) than those calculated for Eddy A (4 km day^{-1}).
304 The deeper depths of modelled eddies were most likely the result of quantifying eddy depths in
305 mA1-mA4 primarily by velocity due to the presence of a mixed layer prior to filament formation.
306 Using velocity observations, Eddy A has a depth of roughly 100 m, which is more comparable to
307 the modelled eddies.
308 Both the simulation and observations contained evidence of upwelling. In the model,
309 isohaline doming and upwelling of slope water dye coincided with formation of a visible spiral
310 pattern (Figure 10, first and second columns). Because slope water dye distributions were
311 unaffected by explicit mixing (e.g., vertical diffusion) of the dye tracer, the presence of elevated
312 slope water dye concentrations within the upper 30m indicates upwelling. Nitrate, phosphate,
313 and silicate were elevated in surface waters within Eddy A relative to surrounding waters when
314 first measured on year-day 132-133 (Figure 4, Supplemental Figure 4), which is consistent with
315 upwelling. Isohaline doming was observed after both filaments had coalesced, on year-day 138-
316 139 (Figure 5), indicating that upwelling was occurring within observed Eddy A. Spiral
317 formation had already begun by year-day 131 (Figure 3). Modelled eddies showed upwelling
318 during spiral formation, indicating that between 2-8 days of upwelling could have occurred prior
319 to our first transect. Thus, the elevated surface nutrients observed in Eddy A could have been due
320 to upwelling.
321 Garvine et al. (1988, 1989) observed two cyclonic slope water eddies similar to that of
322 Eddy A. Each cyclonic slope eddy was bordered by a shelf filament (described as “plumes” in
323 Garvine et al., 1988, 1989) to west and south. Both eddies were adjacent to each other, similar to
324 those in our model. The horizontal and vertical extent of both eddies and accompanying shelf
325 filaments were roughly comparable to those observed in this study, with one of Garvine et al.’s
326 (1988) eddies being twice the diameter of the other (Table 1). Our observed and modelled eddies
327 ranged between their two eddies in size. Both reported eddies had eddy depths similar to
328 observed Eddy A, determined by filament temperatures. The described timeline of their features
329 matched our own, with their transects and SST observations showing similar patterns to our
330 transects for year-days 132-133 and 135 (Figures 3 and 4). Garvine et al. (1988) noted that the
331 region of the shelf-break front to the east of their study region contained no eddies, but did
332 contain frontal meanders. As the front travelled westward, meanders increased in amplitude,
333 culminating in the observed shelf filaments. Garvine et al. (1988) concluded that formation of the
334 shelf filaments contributed to the formation of the cyclonic slope water eddies, in that shelf water
335 was moving offshore and wrapping around slope water. This conclusion is similar to what we
336 have observed and modelled with no major discrepancies. No full spiral or mixing was observed
337 in situ, but their regional satellite imagery (Garvine et al., 1988 – Figure 1) show a few spiral-
338 like features within the MAB. Further analysis indicated that minimal cross-shelf exchange
339 occurred during eddy formation, with offshore and inshore flows being approximately balanced
340 (Garvine et al., 1989). Their conclusion was that significant cross-frontal exchange from their

feature would only occur in the event that the frontal eddies separated from the front (Garvine et al., 1989). The eddies of Garvine et al. (1988, 1989) are the most similar to our Eddy A from past studies at the MAB shelf break. In a broader sense, Eddy A is similar to those observed in frontal spiral eddies elsewhere (e.g., Munk et al., 2000; Pingree, 1978; Pingree, 1979), following a general pattern of shear instability and baroclinic processes within fronts creating spiral eddies. Pingree (1979) notes that the typical diameters of spiral-associated baroclinic shelf-break eddies in the Celtic Sea range from 20 to 45 km, with some larger. Both our diameters and Garvine et al.'s (1988) fall within this range.

Houghton et al. (1986) also observed formation of a frontal slope water eddy with a spiral pattern. However, their eddy was anticyclonic, different from Eddy A observed in this study and those in Garvine et al. (1988). Formation of the eddy based on satellite imagery (Houghton et al., 1986 – Figure 5) showed a shelf filament extending offshore and westward. They argued that frontal baroclinic instability was responsible for the formation of the eddy. However, Houghton et al. (1986) noted that a Gulf Stream warm-core ring had recently passed through the region, which may have resulted in the formation of the anticyclonic eddy through instability of the remnant westward flow within the Slope Sea. Pingree (1978) observed similar anticyclonic spirals forming in various European shelf-break fronts but noted that they were much rarer than cyclonic spirals. Our model generated spirals only in cyclonic eddies, not in anticyclonic eddies. Past studies have shown evidence of both cyclonic spirals (e.g., Garvine et al., 1988) and anticyclonic spirals (e.g., Houghton et al. 1986) at the MAB shelf-break front. Houghton et al. (1986) suggested the influence of a nearby Gulf Stream warm-core ring may be responsible for the rotational direction of their anticyclonic spiral. The possible necessity of secondary flow for anticyclonic spiral formation implies, along with observations and our model results, that anticyclonic spirals may be less common than cyclonic spirals at the MAB shelf-break front.

Another anticyclonic slope water eddy was observed by Gawarkiewicz et al. (2001). Gawarkiewicz et al. (2001) did not observe any spiral pattern in the eddy, but their eddy did remain close to the shelf-break front. Both frontal eddies observed during our cruise and the majority of simulated frontal eddies within this study exhibited this behavior. Their anticyclonic eddy was larger (40 km), slower (0.2 m s^{-1}), and shallower (50 m determined by velocities) than our eddies.

The subduction of shelf filament waters observed during our cruise (Figures 2, 4, and Supplemental Figure 2) were not evident in our model results. The subduction of a thin layer (about 10 m thick) of shelf waters was observed on our transect on year-days 132-133 through 137 (Figure 4). A deep lens of cool, fresh water surrounded by slope waters was seen as late as year-day 139, after contact with the surface had ended (Supplemental Figure 2). Our simulation does not capture the subduction, which may be a result of the relatively low vertical resolution of the model grid at this offshore location. The model vertical layers at the observed depth range of the subducted shelf water have a thickness of 7-8 m, which is too coarse to resolve the thin subducted layer. Observed subducted waters persisted after Eddy A migrated westward and covered relatively large areas (Supplemental Figure 2 year-day 139). Since both observed Eddy A and model Eddies mA1-mA4 remained close to the front without crossing the front, subduction of shelf waters may be important for cross-shelf exchange.

On year-day 132-133, we observed a local nitrate minimum within the slope filament (Figure 2). The temperature-salinity characteristics of the local nitrate minimum were distinct from other waters observed during the same transect but did match waters offshore in the 10-20 m depth interval on year-day 135, where nitrate was similarly low (Supplemental Figure 6). Thus, the most likely source for the local minimum is advection of offshore waters during the initial formation of slope filament. The change in depth between similar nitrate concentrations could suggest downwelling within the slope filament, as seen in the eastern half of the model eddy mA2 on model-day 10.

Chlorophyll was initially equal throughout both filaments of Eddy A when first observed on year-day 132-133 (Figure 4 fifth row). Chlorophyll concentrations increased with time, with elevated chlorophyll within the shelf water filament on year-day 137 and above eddy center on year-day 138-139 (Figure 5). Diatom and copepod abundance were initially higher within the shelf water filament than the slope water filament, likely due to being advected from inshore shelf populations (Figure 4, last two rows). Both diatom and copepod abundance were highest on year-day 138-139, within the center of Eddy A (Figure 5). Surface nitrate, phosphate, and silicate concentrations were lower within the center of Eddy A on year-day 138-139 compared to previous transects (Figure 4, Figure 5, Supplemental Figure 4), coinciding with the increase in chlorophyll, diatoms, and copepods. Combined with the doming isohalines and earlier surface nutrient enhancement during Eddy A formation, it is plausible that we observed upwelling-caused nutrient enhancement, followed by a biological response.

4.2 Eddy B

Our modelled eddies mB1-mB3 qualitatively reproduce formation of anticyclonic flow around a center of cold pool water as measured in Eddy B. Modelled eddies had roughly twice the diameter (20.7±5.1km) compared to observed Eddy B (11 km) (Table 1). Eddy depths (73.3±5.8 m vs. 70 m) and maximum azimuthal velocities (0.27±0.6 m s^{-1} vs 0.2 m s^{-1}) were similar. Modelled westward translational speeds (3.7±0.9 km day^{-1}) were half that of observed Eddy B (8.5 km day^{-1}). The difference between modelled and observed eddy diameters and translational speeds is most likely due to the difference in age between the eddy types. The modelled eddies are larger and slower due to being younger than our observed Eddy B. As the modelled eddies developed, they detach from their originating frontal trough and increase in speed. Presumably, the detached eddies will continue to increase in translational speed while shrinking due to mixing as time passes.

Both observed Eddy B and modelled Eddy mB1-mB3 showed evidence of upwelling of cold pool waters. Upwelling within model eddy mB2 is shown by a mass of detached cold pool water (Figure 9 right column, Figure 11 bottom row). Upwelled shelf dye is originally unevenly distributed due to frontal variability but is later clearly detached from inshore waters and located within the core of the eddy and nearer to the surface. We observed enhanced surface nitrate, phosphate, and silicate within eddy center of Eddy B, which is consistent with upwelling (Figure 6, Supplemental Figure 4).

The closest literature example of eddies similar to our observed Eddy B is from Flagg et al. (1997) (Table 1). Multiple cold pool-associated anticyclonic eddies were observed further south in the MAB compared to our study site, near Cape Hatteras. These eddies contained a layer

of cold pool waters in the upper 50 m of the water column, with additional deeper anticyclonic velocities. Eddy diameters ranged between those of our modelled eddies. Their translational speed (17 km day^{-1}) was double that of our observed Eddy B. Flagg et al. (1997) noted that such eddies could not be formed locally, due to constraints in local bathymetry and hydrographic characteristics, and so must have travelled a significant distance from the north. Both higher chlorophyll-normalized primary productivity and higher oxygen saturation were measured within one of the eddies compared to surrounding shelf waters, with Flagg et al. (1997) hypothesizing that a nutrient-enhanced bloom had occurred 1-2 weeks prior to observation. Chlorophyll was locally high on the periphery of the observed eddy, similar to what we observed in Eddy B. While much farther south than our study location, the characteristics of their eddies match our own. By our earlier estimation, the difference in translational speeds places the age of our observed Eddy B between those of our modelled eddies and those observed by Flagg et al. (1997), which in and of itself indicates the persistence of cold pool-associated anticyclonic eddies. The eddies observed by Flagg et al. (1997) did not cross the front but did serve as a mechanism for southward movement of cold pool water. This could have implications for the eventual fate of such eddies, perhaps as a mechanism to preserve upstream water characteristics while the frontal eddies move downstream along the shelf edge. Additionally, the eddies observed by Flagg et al. (1997) were highly productive, indicating that our observed anticyclonic eddies could be similarly productive.

Historic satellite imagery of our section of the MAB (Garvine et al., 1988 – Figure 1) shows at least one feature that appears to have a filament of warmer waters (frontal or slope in origin) wrapping anticyclonically around shelf water, similar to that of our model Eddy mB2. Anticyclonic vorticities were observed within shelf filaments bordering eddies similar to our Eddy A (β plume in Garvine et al., 1989) that matched our early modelled eddy formation. We did not see evidence of recirculation within the plume as concluded by Garvine et al. (1989), but we did see similar anticyclonic behavior. In our modelled eddies, this anticyclonic behavior developed into anticyclonic shelf eddies. One major difference was that the β plume did not contain cold pool water, which may be due to the relatively early state of the feature.

Our model results, as well as the observations of repeated anticyclonic cold pool eddies by Flagg et al. (1997), imply that features similar to Eddy B should be relatively common along the MAB shelf-break front. Model Eddy mB1 crossed the front into the Slope Sea and model Eddy mB2 drew near-frontal water inshore away from the front, indicating that eddies similar to Eddy B may contribute in multiple fashions to cross-frontal water exchange.

Chlorophyll was enhanced in the periphery of Eddy B, and VPR-measured diatoms and copepods concentrations were higher within the eddy center for the duration of our measurements (Figure 6). The lack of elevated chlorophyll in the center of Eddy B may have been caused by sustained high grazing on phytoplankton smaller than the diatom chains resolved by the VPR, as our observation likely occurred during a late stage of the biological response in Eddy B. Other possible reasons for the separation between observed chlorophyll enhancement and elevated diatom abundance within Eddy B include that the diatoms imaged by the VPR (>100μm in diameter) were a small percentage of overall chlorophyll and that the diatoms observed had higher carbon:chlorophyll ratios compared to phytoplankton in the periphery. Observations also showed higher abundance of diatoms and copepods further inshore than in the

center of Eddy B. Therefore, both may be more abundant in the center of Eddy B as a result of advection from inshore. Another possible explanation for the higher copepod abundance within the center of Eddy B is due to aggregation.

4.3 Interpretation of biological results

The focus of this study has been on the formation of two eddies characterized by different water masses and biogeochemical properties. Within the two features discussed, there were changes in nutrients, chlorophyll, diatom chains, and copepods over time. Of course, these changes occurred in the context of a dynamic region that contains patchiness on many scales. For example, diatom chain and copepod abundances fluctuate inshore and offshore of our eddies during the course of our observations (Figures 4-7, Supplemental Figures 2 and 5). These fluctuations were most likely the result of advection, since the time between successive transects was insufficient for the rapid changes in observed abundance. The greater patchiness of copepod distributions is consistent with the tendency for flattening of the variance spectrum in higher trophic levels (e.g., Abraham, 1998; Mackas and Boyd, 1979).

We also note that the distributions for chlorophyll did not always align with those of diatom chains, particularly for Eddy B (Figure 6). The primary reason for this is that the large diatom chains (>200μm) measured in this study were a small fraction of the phytoplankton community in the shelf waters and near the front (e.g., Archibald, 2021; Stevens et al., 2023). However, even at relatively low abundances, diatoms can play an important ecological role (Smetacek, 1999).

4.4 Relation to frontal instabilities

Formation of the observed features Eddy A and Eddy B in the ocean are presumably induced by frontal instabilities of the shelf-break front. This study has primarily focused on providing a descriptive analysis of observations and model results rather than the mechanisms generating frontal instabilities or the specific conditions necessary for frontal instabilities to develop into the features presented herein. To characterize the eddies, we estimate the Burger number for our observed eddies, $S = (NH/fL)^2$, which measures the ratio of the energy conversion associated with barotropic to baroclinic instability during the process of frontal eddy formation (Zhang and Gawarkiewicz, 2015). Here, N is a scale of the buoyancy frequency, H is the vertical extent of the eddy, $f = 10^{-4}$ s^{-1} is the Coriolis parameter, and L is the eddy diameter (H and L from Table 1). The buoyancy frequency was calculated as a median of 5m depth averaged bins for year-days 132-133 (Eddy A, Figure 2 left column) and 142-143 (Eddy B, Figure 2 right column) spanning the vertical and horizontal extent of each feature (H: 0-70m, L: white lines in Figure 2) for calculating the Burger Number. The Burger number for Eddy A was $S = 0.0412$ ($N = 0.0087$ s^{-1}, $H = 70$ m, $L = 30$km) and $S = 0.1358$ for Eddy B ($N = 0.01116$ s^{-1}, 70 m, $L = 22$ km). This indicates Eddy A and Eddy B were likely to have been formed by baroclinic frontal instabilities, and the contribution of barotropic instability was relatively higher in forming Eddy B than Eddy A.

Barotropic and baroclinic instabilities of the MAB shelf-break front are known to generate large-amplitude meanders (Lozier et al., 2002) with patches of high and low vorticity on either side of the front (Zhang and Gawarkiewicz, 2015), causing both upwelling and

downwelling near the front. Nutrient-rich water upwelled during the subsequent eddy formation could potentially increase nutrient availability in the euphotic zone. Our modeled anticyclonic eddies (mB1-3) showed patchy shelf water dye distributions prior to eddy formation, which likely result from submesoscale variability induced by the early-stage frontal instability (Figure 11). It appears that the early-stage variability also upwelled shelf water dye prior to detachment of cold pool waters in model eddies similar to Eddy B. Details of the dynamical connections between those frontal submesoscale processes and enhancement of nutrients on the scale of eddies remain unknown. Determining the precise mechanisms of the frontal instabilities impacting the eddies presented in this study are left for future work.

5. Conclusions

Frontal eddies have long been observed in satellite imagery near the MAB shelf-break front, but relatively few have been observed in situ. In this study, we analyzed observations of two eddies, a cyclonic spiral eddy located seaward of the front and an anticyclonic eddy shoreward of the front. Despite having differing rotational directions, both eddies showed evidence of upwelling and nutrient enhancement. Based on our model simulations, we infer that the cyclonic eddy contained locally driven upwelling that occurred for the duration of observations. The model also illustrates how the anticyclonic eddy was formed while cold pool water upwelling occurred along the front, detaching from its parent water mass. Surface nutrient enhancement occurred only during eddy formation and was not replenished during the life of the eddy – consistent with the model predictions of upwelling. Chlorophyll, diatom, and copepod enhancements occurred within both eddies, indicating possible biological responses to upwelled nutrients. Satellite imagery and prior studies suggest that frontal eddies similar to those observed herein are abundant within the MAB shelf-break frontal region. Both our observations and model results indicate that both eddy types may persist for more than a month, indicating that both eddy types may have significant impacts on biological communities near the front.

6. Acknowledgements

We thank Olga Kosnyrev for data stewardship and Philip Alatalo for assistance with plankton image analysis. This work was completed as a component of the Shelf-break Productivity Interdisciplinary Research Operation at the Pioneer Array (SPIROPA) project, funded by the National Science Foundation (OCE-1657803, OCE-1658054, OCE-2322676) and the Dalio Explorer Fund. We additionally thank our SPIROPA colleagues for overall assistance and support, and the captain, crew, and marine technicians of the *NOAAS Ronald H. Brown* for their assistance and support at sea. We also thank the OOI program for their operation of the Pioneer Array, which provided valuable context for this study.

7. Data availability statement

SPIROPA CTD, DAVPR, and nutrient bottle data are archived at the Biological and Chemical Oceanography Data Management Office (BCO-DMO) project page: https://www.bco-dmo.org/project/748894 (McGillicuddy et al., 2020). AVHRR sea surface temperature are available from the Mid-Atlantic Regional Association Coastal Ocean Observing System (MARCOOS) at https://tds.maracoos.org/thredds/catalog/ARCHIVE-SST.html (2019). All figures were created in Matlab version 2020b.

References

Abraham, E (1998). The generation of plankton patchiness by turbulent stirring. *Nature*, 391, 577–580.

Archibald, K.M. (2021). The role of zooplankton in regulating carbon export and phytoplankton community structure: integrating models and observations. Ph.D. thesis, Massachusetts Institute of Technology, Cambridge MA USA, and Woods Hole Oceanographic Institution, Woods Hole MA USA.

Beardsley, R.C., Flagg, C.N. (1976). The water structure, mean currents, and shelf/slope water front on the New England continental shelf. *Mem Soc. Roy. Sci. Liege*, 6, 209–225.

Chen, K., He, R. (2010). Numerical investigation of the Middle Atlantic Bight shelfbreak frontal circulation using a high-resolution ocean hindcast model. *J. Phys. Oceanogr*., 40, 949–964.

Davis, C.S., Hu Q., Gallager S., Tang X., Ashjian C.J. (2004). Real-time observation of taxa-specific plankton distributions: An optical sampling method. *Mar. Ecol. Progr. Ser*., 284, 77-96.

Davis, C.S., Thwaites, F.T., Gallager, S.M., Hu, Q. (2005). A three-axis fast-tow digital Video Plankton Recorder for rapid surveys of plankton taxa and hydrography. *Limnol. Oceanogr. Meth*., 3, 59-74.

Dewar, W.K. (1986). Mixed layers in Gulf Stream rings. *Dyn. Atmos. Oceans,* 10, 1–29.

Flagg, C.N., Wallace, D., Kolber, Z. (1997). Cold anticyclonic eddies formed from cold pool water in the southern Middle Atlantic Bight. *Cont. Shelf Res.,* 17(15), 1839-1867.

Garvine, R.W., Wong, K.-C., Gawarkiewicz, G.G., McCarthy, R.K. (1988). The morphology of shelfbreak eddies. *J. Geophys. Res.*, 93(C12), 15593-15607.

Garvine, R.W., Wong, K.-C., Gawarkiewicz, G.G. (1989). Quantitative properties of shelfbreak eddies. *J. Geophys. Res.*, 94(C10), 14475-14483.

Gawarkiewicz, G., Bahr, F., Beardsley, R.C., Brink, K.H. (2001). Interaction of a Slope Eddy with the Shelfbreak Front in the Middle Atlantic Bight. *J. Phys. Oceanogr*., 31, 2783–2796

Gawarkiewicz, G., Brink, K.H., Bahr, F., Beardsley, R.C., Caruso, M., Lynch, J.F., Chiu, C.-S. 2004. A large-amplitude meander of the shelfbreak front during summer south of New England: Observations from the Shelfbreak PRIMER experiment. *J. Geophys. Res*., 109.

Hirzel, A.J. (2023). Physical and biological processes at the Middle Atlantic Bight shelf-break front. Ph.D. thesis, Massachusetts Institute of Technology, Cambridge, MA, USA, and Woods Hole Oceanographic Institution, Woods Hole, MA, USA.

Houghton, R.W., Olson, D.B., Celone, P.J. (1986). Observation of an anticyclonic eddy near the continental shelf break south of New England. *J. Phys. Oceanogr.,* 16, 60-71.

Houghton, R.W., Schlitz, R., Beardsley, R.C., Butman, B., Chamberlin, J.L. (1982). The Middle-Atlantic Bight cold pool: evolution of the temperature structure during summer 1979. *J. Phys. Oceanogr.*, 12, 1019–1029.

Kennelly, M.A., Evans, R.H., Joyce, T.M. (1985). Small-scale cyclones on the periphery of a Gulf Stream warm-core ring. *J. Geophys. Res.,* 90(C5), 8845-8857.

Lentz, S.J. (2003), A climatology of salty intrusions over the continental shelf from Georges Bank to Cape Hatteras. *J. Geophys. Res.*, 108(C10), 3326.

Lentz, S.J. (2017). Seasonal warming of the Middle Atlantic Bight cold pool. *J. Geophy. Res.: Oceans,* 122, 941–954.

Linder, C.A., Gawarkiewicz, G. (1998). A climatology of the shelfbreak front in the Middle Atlantic Bight. *J. Geophys. Res*., 103, 18,405–18,423.

Loder, J., Shore, J., Hannah, C., Petrie, B.D. (2001). Decadal-scale hydrographic and circulation variability in the Scotia–Maine region. *Deep-Sea Res. Pt. II*, 48, 3-35.

Lozier, M.S., Reed, M.S.C., Gawarkiewicz, G.G. (2002). Instability of a shelfbreak Front. *J. Phys. Oceanogr.,* 32, 924–944.

Mackas, D.L., Boyd, C.M. (1979). Spectral analysis of zooplankton spatial heterogeneity. *Science*, 204, 62–64.

McGillicuddy, D.J., Smith, W.O., Stanley, R., Turner, J., Petitpas, C., Sosik, H.M., Zhang, W.G. (2020). Project: collaborative research: shelfbreak frontal dynamics: mechanisms of upwelling, net community production, and ecological implications. BCO-DMO, 2020-09, https://www.bco-dmo.org/project/748894

Mid-Atlantic Regional Association Coastal Ocean Observing System (MARCOOS) (2019). MARCOOS – THREDDS archive SST. THREDDS, 2019-10-18, https://tds.maracoos.org/thredds/catalog/ARCHIVE-SST.html

Munk, W., Armi, L., Fischer, K., Zachariasen, F. (2000). Spirals on the sea. *Proc. R. Soc. Lond. A*, 456, 1217-1280

Pickart, R.S., Torres, D., McKee, T.K., Caruso, M., Przystup, J.E. (1999). Diagnosing a meander of the shelf break current in the Middle Atlantic Bight. *J. Geophys. Res.,* 104.

Pingree, R.D. (1978). Cyclonic eddies and cross-frontal mixing. *J. Mar. Biol. Ass. U.K.*, 58, 955-963.

Pingree, R.D. (1979). Baroclinic eddies bordering the Celtic Sea in late summer. *J. Mar. Biol. Ass. U.K.*, 59, 689-698.

Ryan, J.P., Yoder, J.A., Cornillon, P.C. (1999a). Enhanced chlorophyll at the shelfbreak of the Mid-Atlantic Bight and Georges Bank during the spring transition. *Limnol. Oceanogr*., 44(1), 1–11.

Ryan, J.P., Yoder, J.A., Barth, J.A., Cornillon, P.C. (1999b). Chlorophyll enhancement and mixing associated with meanders of the shelf break front in the Mid-Atlantic Bight. *J. Geophys. Res.,* 104(C10), 23479-23493.

Shchepetkin, A.F., McWilliams, J.C. (2008). Computational kernel algorithms for fine-scale, multiprocess, long-term oceanic simulations. *Handbook of Numerical Analysis. XIV: Computational Methods for the Atmosphere and the Ocean*, Ciarlet, P.G., Temam, R., Tribbia, J. (eds.), *Elsevier*, 121–183.

Smetacek, V. (1999). Diatoms and the ocean carbon cycle. *Protist*, 150(1), 25-32.

Spall, M.A., Thomas, L.N., (2016). Downfront winds over buoyant coastal plumes. *J. Phys. Oceanogr.*, 46, 3139–3154.

Stevens, B.L.F., Crockford, E.T., Peacock, E.E., Neubert, M.G., Sosik, H.M. (2023). Temperature regulates *Synechococcus* population dynamics seasonally and across the continental shelf. *Limnol. Oceanogr. Lett.*

Williams, R.G. (1988). Modification of ocean eddies by air-sea interaction. *J. Geophys. Res. Oceans,* 93, 15523–15533.

Zhang, W.G., Gawarkiewicz, G.G., McGillicuddy, D.J., Wilkin, J.L. (2011). Climatological mean circulation at the New England shelf break. *J. Phys. Oceanogr*., 41, 1874–1893.

Zhang, W.G., Gawarkiewicz, G. (2015). Length scale of the finite-amplitude meanders of shelfbreak fronts. *J. Phys. Oceanogr.*, 45, 2598-2620.

Table 1: Key differences between Eddy A and Eddy B, along with citations of similar features. Values were estimated from our observations for our eddies. Cited numbers include values estimated from figures. Eddies α_c and β_c are two cyclonic features described in Garvine et al. (1988).

	Eddy A	Modelled Eddies mA1-mA4	Garvine et al., 1988 (Similar to A)	Eddy B	Modelled Eddies mB1-mB3	Flagg et al.,1997 (Similar to B)
Core Water Mass:	Slope			Shelf		
Rotation:	Cyclonic			Anticyclonic		
Upwelled Water Mass:	Slope			Cold Pool		
Radius (km):	15	mA1: 17 mA2: 20 mA3: 18 mA4: 20	α_c: 10 β_c: 20	11	mB1: 22 mB2: 25 mB3: 15	15 - 22.5
Horizontal Ellipticity:	0.9	mA1: 0.9 mA2: 0.9 mA3: 1.0 mA4: 0.9	α_c: 0.9 β_c: 1	0.7	mB1: 0.8 mB2: 0.7 mB3: 0.8	~ 1
Maximum Azimuthal Velocity (m $s^{-1)}$:	0.4	mA1: 0.4 mA2: 0.4 mA3: 0.4 mA4: 0.4	Drifter Velocities: α_c: ~0.2 β_c: ~0.2	0.2	mB1: 0.3 mB2: 0.3 mB3: 0.2	0.25
Translation Speed (km day^{-1}):	4	mA1: 3.9 mA2: 2.8 mA3: 2.2 mA4: 3	4.8	8.5	mB1: 2.7 mB2: 4.5 mB3: 4	17
Eddy Depth (m):	70	mA1: 120 mA2: 140 mA3: 120 mA4: 120	α_c: 50 β_c: 70	70	mB1: 70 mB2: 70 mB3: 80	60

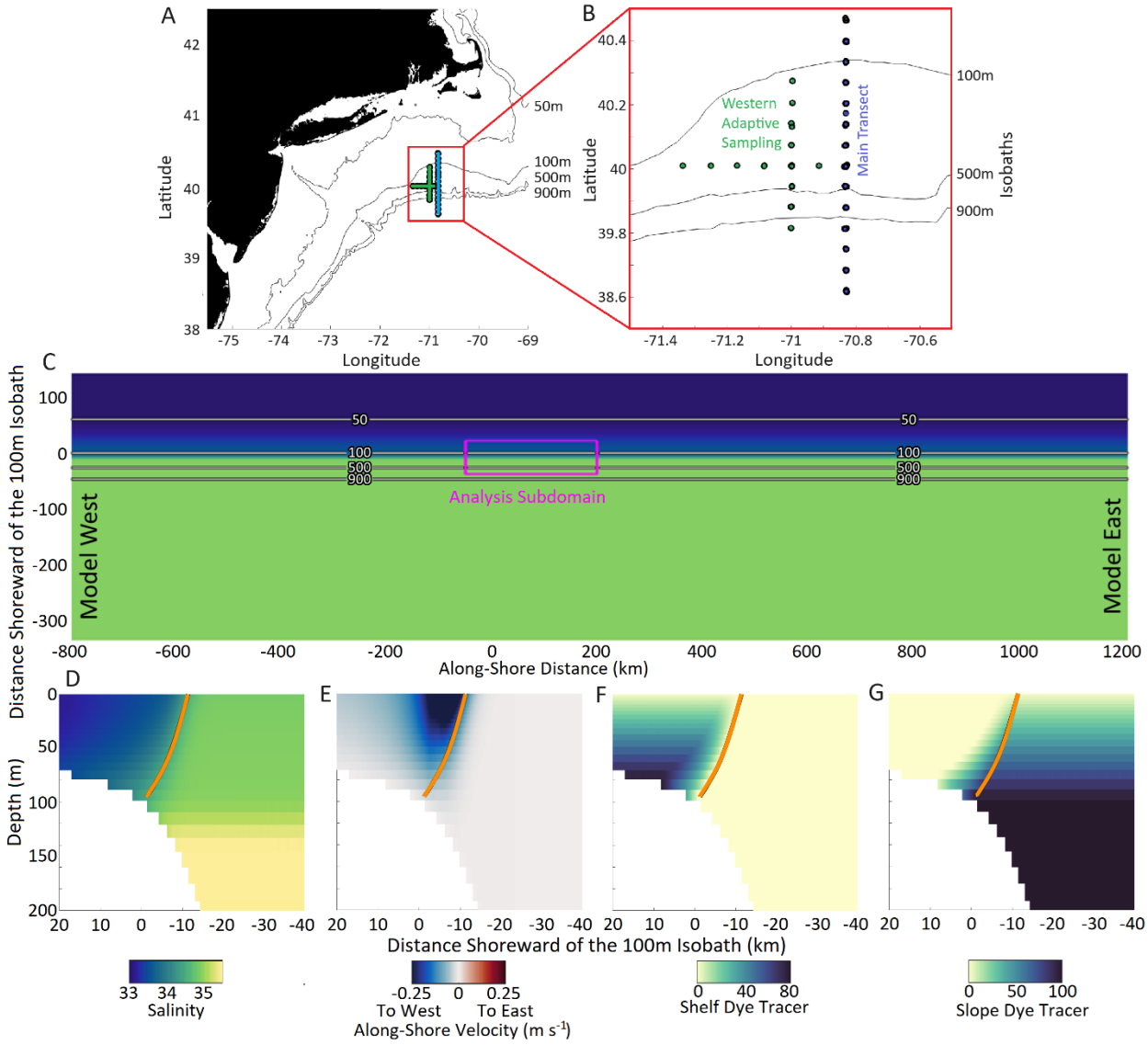

Figure 1: A, B) Location of CTD stations and regional isobaths (black contours). Blue markings signify the main north-south transect and green markings signify transects west of the main transect (Year-days 138-139 and 144). C) Overhead view of the model domain with isobaths (black and white contours). The magenta box is the analysis subdomain. D-G) Initial modelled salinity, along-shore velocity, and dye concentrations along a transect in the cross-shelf direction (third row). The orange contour denotes the 34.5 isohaline. All modelled variables are initially uniform in the along-shelf direction.

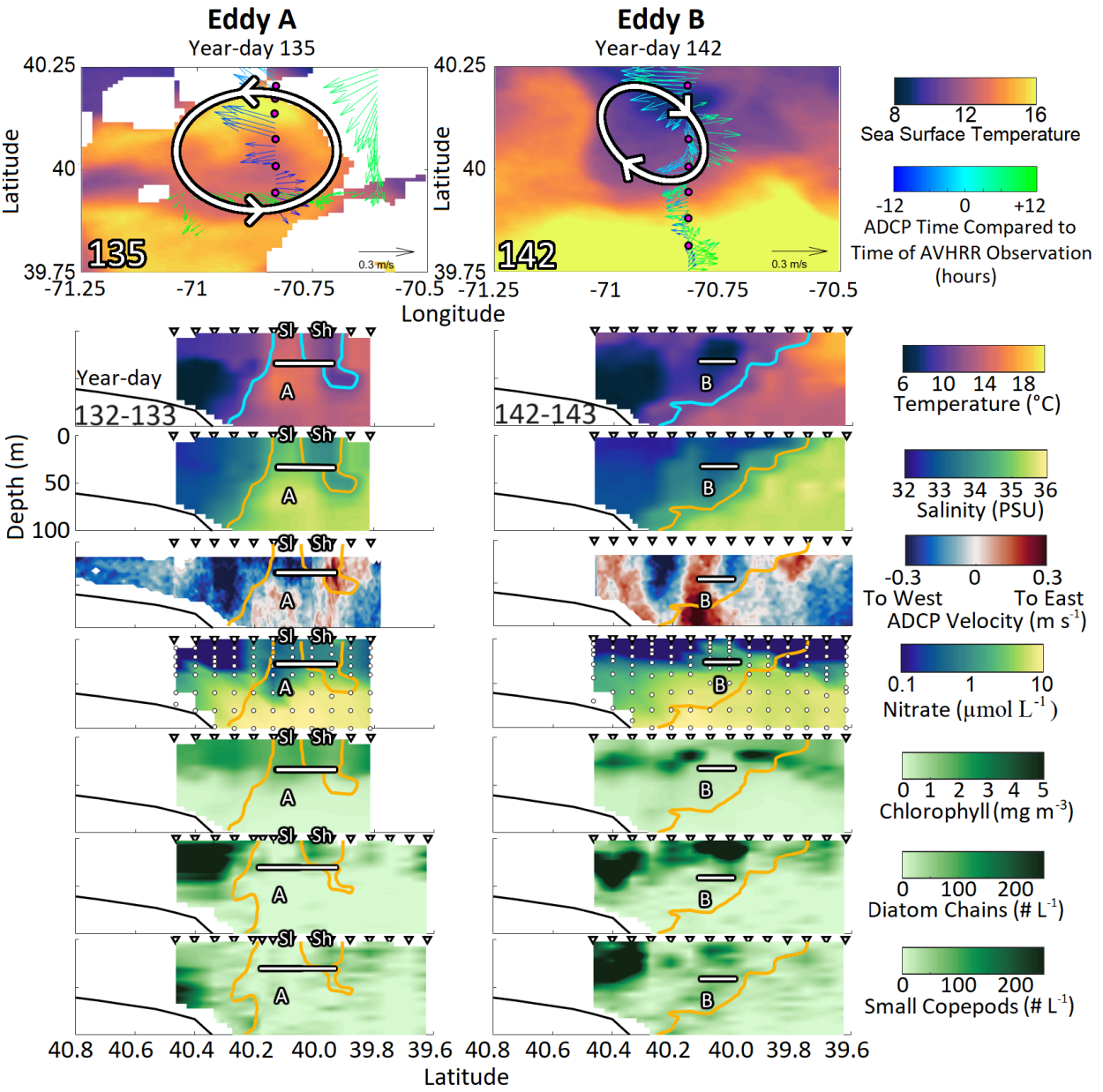

Figure 2: Sea surface temperature and transect observations of Eddy A and Eddy B. The first row shows AVHRR sea surface temperature with approximate eddy positions overlaid. Magenta dots represent CTD stations sampled within 12 hours (before or after) of the SST image. Detided ADCP data, averaged from 17-49 m, collected within 12 hours (before and after) of the SST image are overlaid. The lower 3 rows are CTD north-south transects for temperature, salinity, and east-west ADCP velocity. Transect station locations are marked by triangles. Teal and orange lines denote the 34.5 isohaline. In all plots, the approximate locations of eddies A or B are shown by white lines. "Sl" and "Sh" denote the locations of the slope and shelf water filaments respectively for Eddy A (left column).

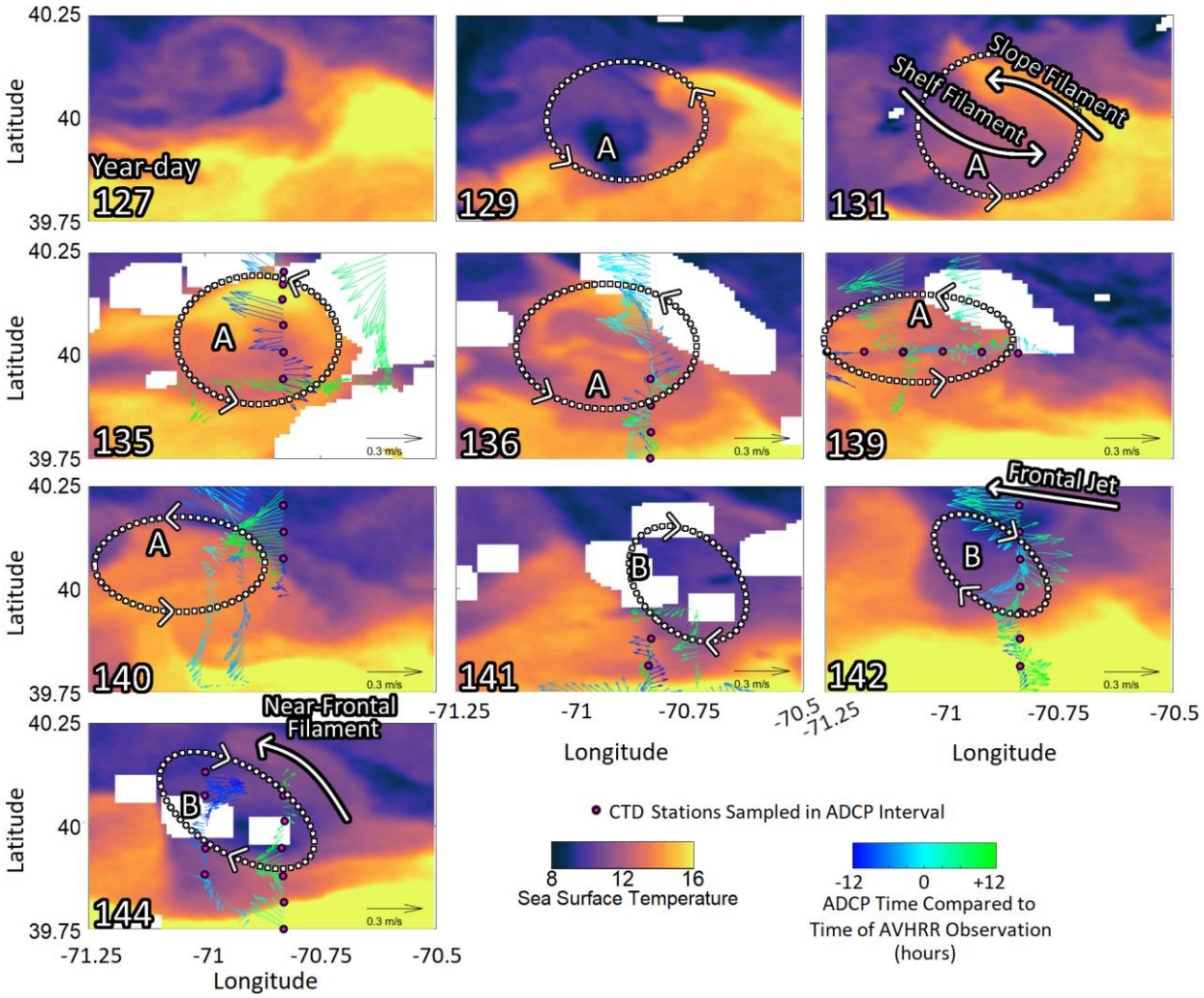

Figure 3: AVHRR sea surface temperature with approximate eddy position overlaid. Magenta dots represent CTD stations sampled within 12 hours (before or after) of the SST image. Overlaid are detided ADCP velocities, averaged over the depth range of 17-49 m, collected within 12 hours (before and after) of the SST image. Circles denote approximate borders of eddies A and B and arrows denote the direction of eddy rotation. Eddy borders are drawn using all available information (Figures 4-7, Supplemental Figures 1-5) as SST alone was insufficient to characterize the eddies, particularly Eddy B which was identified primarily by subsurface characteristics. Labelled arrows denote features discussed in the text: the two filaments associated with Eddy A (year-day 131), frontal jet velocities, which are distinct from velocities of Eddy B (year-day 142), and the filament of near-frontal waters near Eddy B (year-day 144).

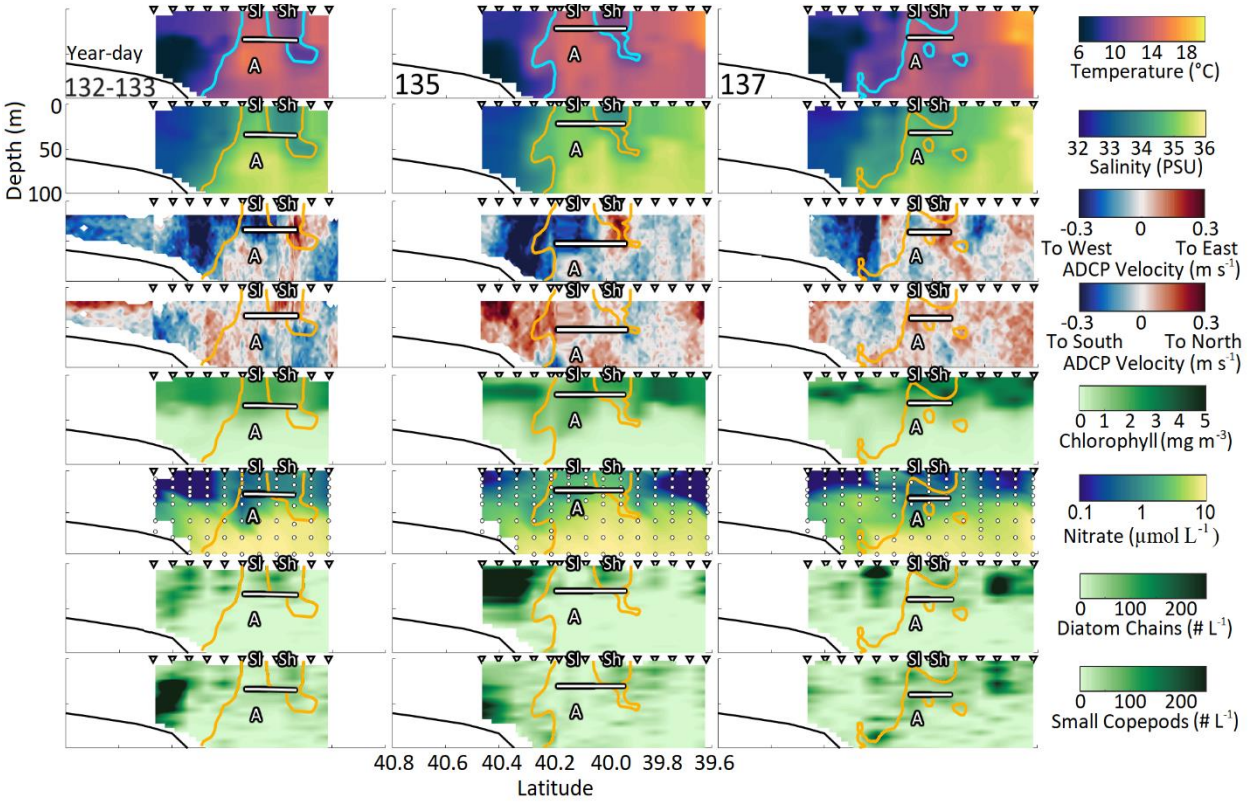

Figure 4: All north-south transects for Eddy A. Location of the eddy is denoted by white lines. "Sl" and "Sh" denote the locations of the slope and shelf water filaments respectively. Teal (first row) and orange (all other rows) contours indicate the location of the 34.5 isohaline. Black triangles show the locations of sampled stations. ADCP data was sampled continuously while underway. White circles represent bottle sample depths and locations.

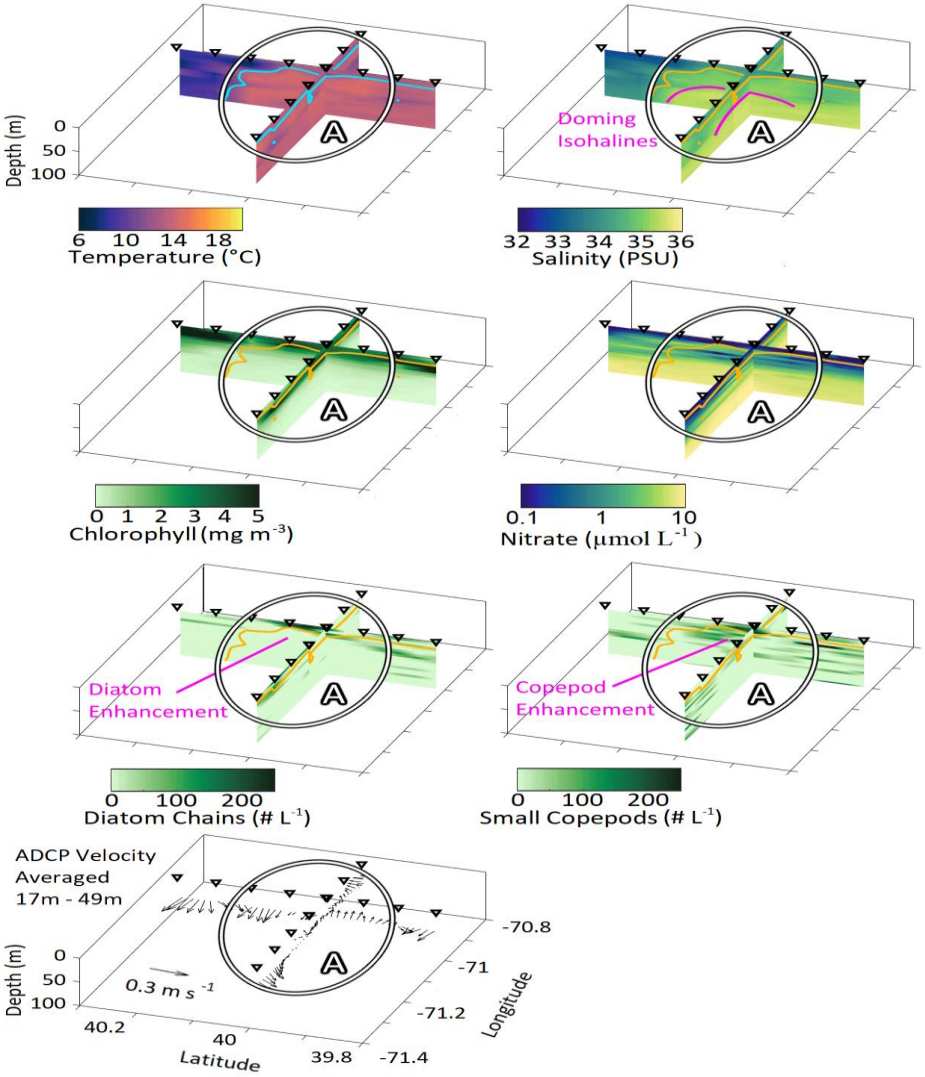

Figure 5: Adaptive sampling of Eddy A west of the main transect on year-day 138-139. Transects are presented from a point of view looking down from west-southwest. White circles delineate the approximate borders of Eddy A. Teal (first plot) and orange (all others) contours indicate the location of the 34.5 isohaline. Black triangles show the locations of sampled stations. ADCP measurements are averaged over the depth range of 17-49 m and plotted at a depth of 40 m. Magenta labels highlight some of the eddy characteristics mentioned within the text.

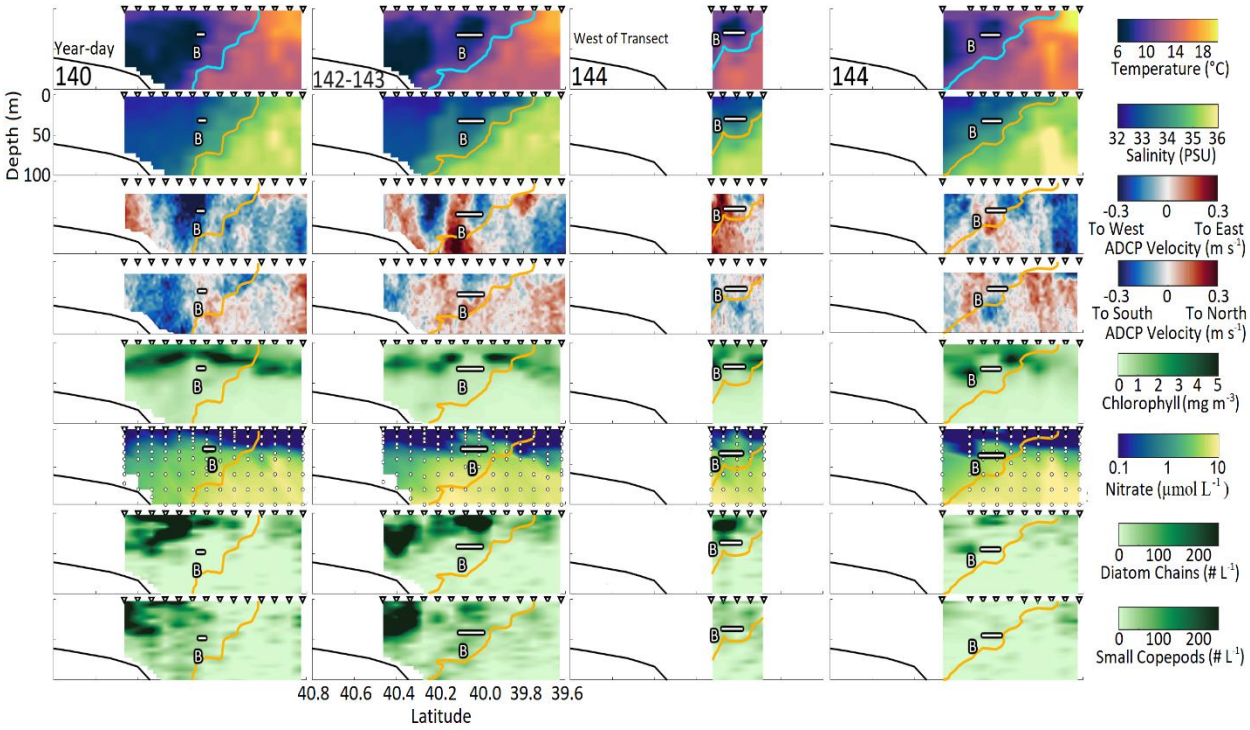

Figure 6: All north-south transects for Eddy B. The first, second, and fourth columns were taken along the same longitude, while the third column was located to the west. Location of the eddy is denoted by white lines. Teal (first row) and orange (all other rows) contours indicate the location of the 34.5 isohaline. Black triangles show the locations of sampled stations. ADCP data was sampled continuously while underway. White circles represent bottle sample depths and locations.

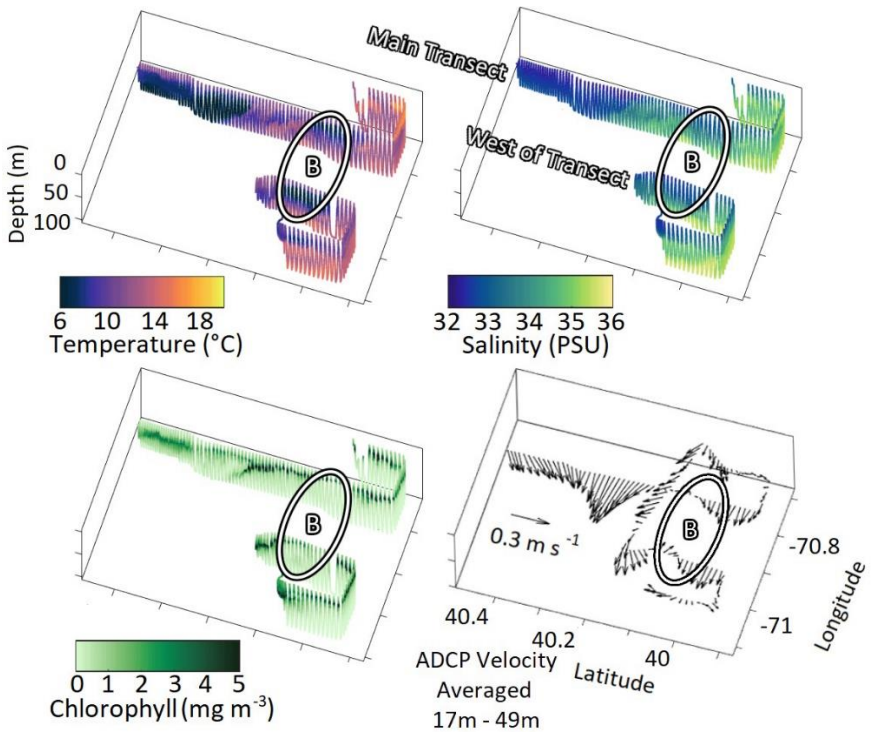

Figure 7: Two VPRII tows on year-day 143. Transects are presented from a point of view looking down from west-southwest. White lines show the extent of Eddy B. ADCP measurements are averaged over the depth range of 17-49 m and plotted at a depth of 40 m. Transect labels (upper right) denote north-south transects resampled on year-day 144 (Figure 6).

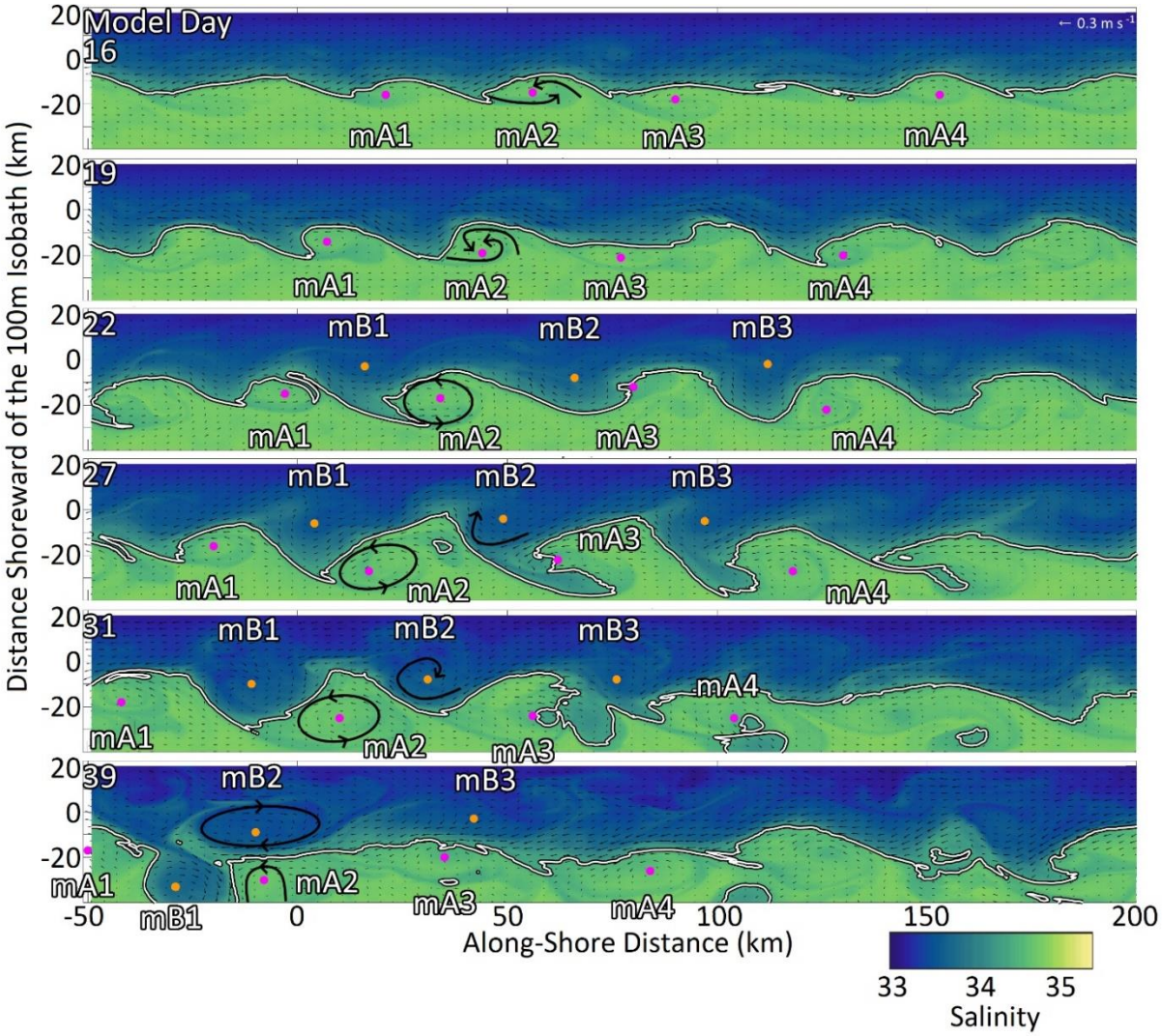

Figure 8: Modelled salinity (color) and horizontal velocity (vectors with scale in upper right of top plot) at 30 m depth. Four Eddy A-like features (mA1-mA4, centers marked in magenta) and three Eddy B-like features (mB1-mB3, centers marked in orange) were tracked over time in this study. Centers are marked based on full water column analysis, not just the presented depth slice. The features described in detail herein are Eddies mA2 and mB2. Overlaid in black is the flow pattern described within the text and depicted in greater detail in Figures 10 and 11. The shelf-break front is represented by the 34.5 isohaline (white contours).

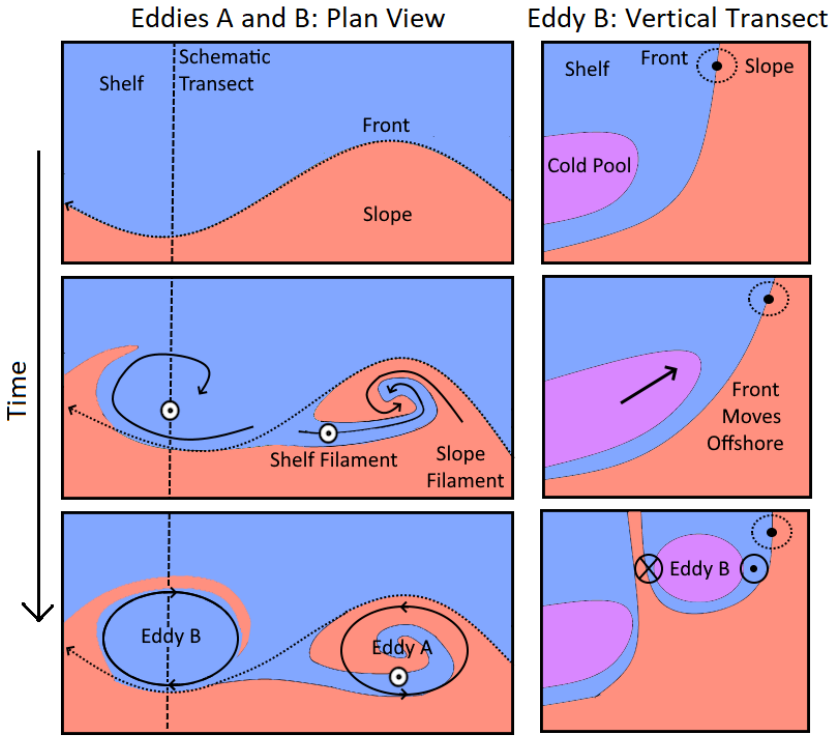

Figure 9: A simplified schematic showing the formation mechanisms of Eddy A and B. Though presented side-by-side for the sake of comparison, Eddy B formation occurs later than Eddy A formation within our simulation. The left panel shows a top view of the formation process. Velocity 'targets' in the left column represent zones of upwelling. The right column shows the upwelling process at the interior of Eddy B. The dotted line in the left column is represents the transect shown on the right.

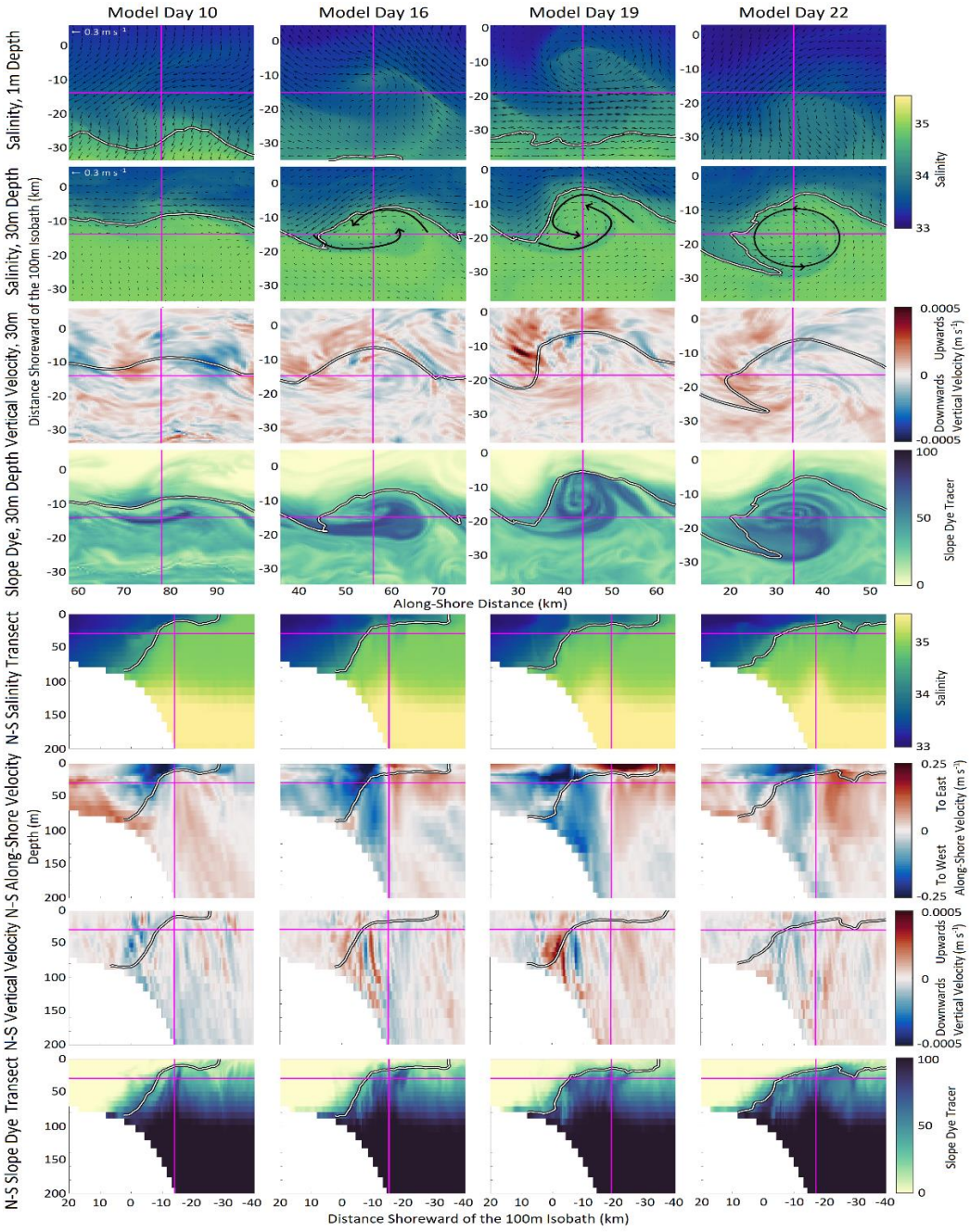

Figure 10: Magnified model results centered on Eddy mA2. The first three rows are horizontal z-slices of fixed depth (first row: 1m, next three rows: 30 m), with a 40 x 40 km subdomain centered on the eddy center. Horizontal velocity is overlaid on salinity in the first two rows (velocity scale in leftmost plots). The latter four rows are cross-shelf transects along the vertical magenta line shown in the first three rows, with expanded inshore and offshore coverage. The vertical magenta lines in the latter three rows mark the location of the horizontal magenta line in the first three rows. The horizontal magenta lines in the latter plots represent 30 m depth. Overlaid on the second row in black is the Eddy A formation process described within the text. White contours are the 34.5 isohaline, representing the shelf-break front. Vertical velocity (third and sixth rows) and their respective salinity contours are averaged over 24 hours.

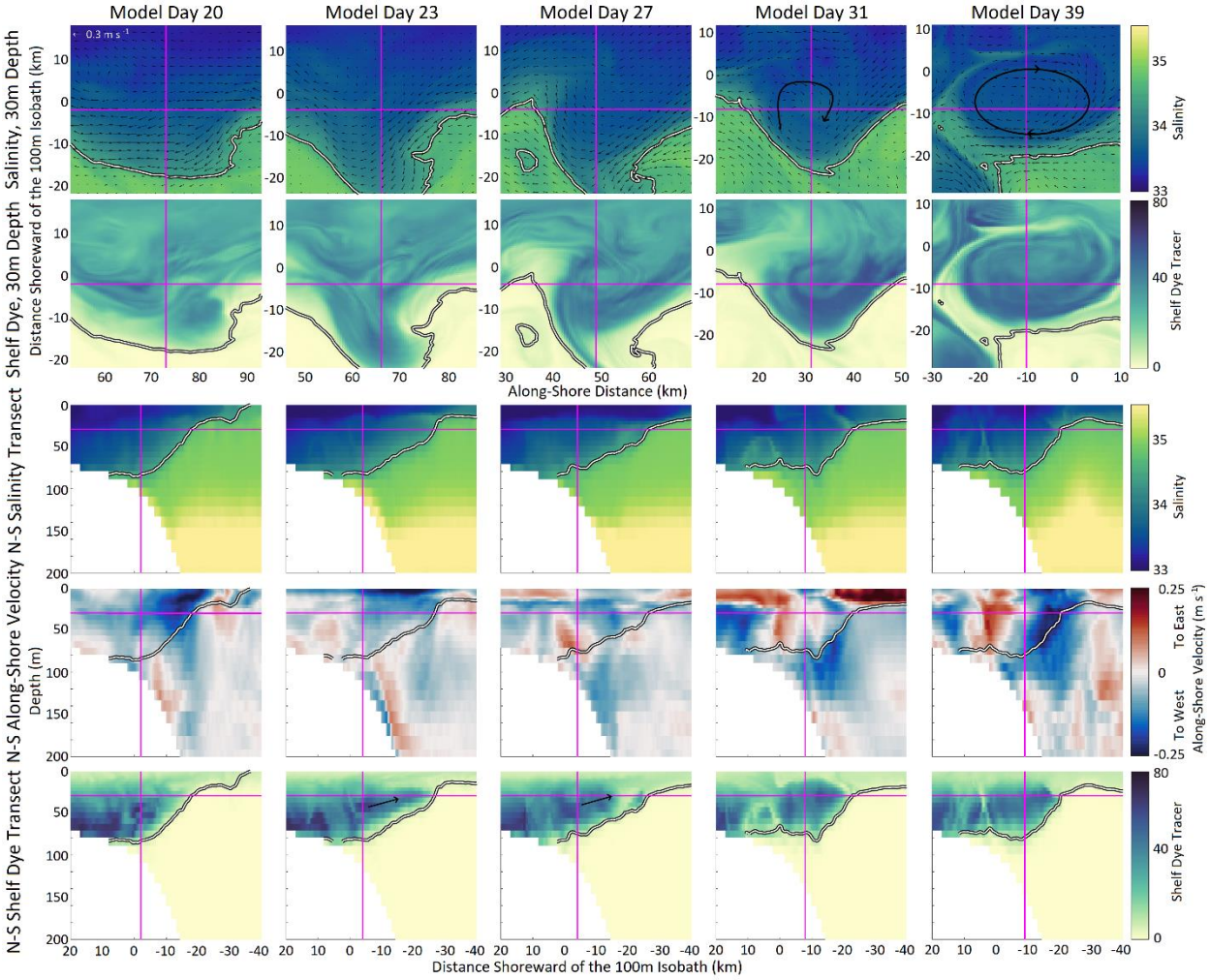

Figure 11: Magnified model results centered on Eddy mB2. The first three rows are horizontal z-slices at 30 m depth, with a 40 x 40 km subdomain centered on the eddy center. Horizontal velocity is overlaid on salinity in the first rows (velocity scale in leftmost plots). The latter three rows are cross-shelf transects along the vertical magenta line shown in the first two rows, with expanded inshore and offshore coverage. The vertical magenta lines in the latter three rows mark the location of the horizontal magenta line in the first three rows. The horizontal magenta lines in the latter plots represent 30 m depth. Overlaid on the second row in black is the Eddy B formation process described within the text. White contours are the 34.5 isohaline, representing the shelf-break front.